Modeling droplets swelling and escape in double emulsions using population balance equations

Behnam Khadem, Nida Sheibat-Othman

Modeling droplets swelling and escape in double emulsions using population balance equations

Behnam Khadem[1], Nida Sheibat-Othman[*]

University of Lyon, Université Claude Bernard Lyon 1, CNRS, LAGEPP UMR 5007, F-69100, Villeurbanne, France

[*]Corresponding author: nida.otham@univ-lyon1.fr

Abstract

Monitoring the physical stability of double emulsions is considered in this work. A coupled population balance equation model for the inner and outer droplets is developed. The model involves a sub-model describing swelling of the inner, and so of the outer, droplets and a sub-model describing the escape of the inner droplets. The swelling phenomena is governed by the osmotic and Laplace pressures while the inner droplet escape rate is governed by the balance of the surface and viscous forces of the droplets. Experimental investigations demonstrate the usefulness of the model and its capability to describe the evolution of the inner and outer droplets size distributions and the release rate during storage of the double emulsions.

Keywords: Double emulsions, Population balance modelling, Swelling, Escape, Release.

1. Introduction

Double emulsions are essential for the production of low-fat foods [1], the encapsulation of pharmaceutical active agents [2], or the extraction of substances such as in wastewater treatment industry [3]. Almost a century after their first observation by Seifriz et al. (1925) [4], double emulsions preparation and stability still represent several challenges. Double emulsions are commonly prepared in a two-step method which was proposed by Matsumoto et al. (1976) [5]. In this method, a primary emulsion is prepared in a first step under high shear, generating a dispersion of small droplets, called inner (or micro-) droplets, that is then dispersed into an external phase under lower shear to obtain bigger outer droplets (also called globules, or

macro-droplets). The droplets size and the encapsulation efficiency are two key parameters of the product quality in such emulsions.

The stability of double emulsions has been subject of many studies in recent years, including investigations of the effects of the emulsification device [6], the surfactants nature and concentration [7–9] and the inner and outer droplets size [6,9]. During storage, the phenomena that may take place are inner or outer droplets coalescence, Ostwald ripening leading to droplets growth, shrinkage or swelling of the inner droplets and thus of the outer droplets [10–15] and the release of the encapsulated substance [3,7,15–19]. Concerning the release, on one hand, it may occur at the inner droplet level, also called escape. This phenomena is described by the coalescence of inner droplets with the external continuous phase through the surface of the outer droplets. The release may, on the other hand, take place at a molecular level by diffusion of the encapsulated substance until reaching the external phase, without causing film rupture. Concerning the shrinkage or the swelling phenomena, they take place due to the osmotic pressure gradient. The swelling phenomena may ultimately lead to swelling-breakdown, i.e. the expulsion of the inner droplets out of the outer droplet [15]. This phenomenon takes place either gradually, or more abruptly leading to the disintegration of the outer droplet [20], herein called “overswelling-breakdown”. In this work, both the swelling and escape phenomena (i.e. the release by coalescence) will be investigated experimentally and theoretically, until the onset of the overswelling-breakdown phenomena.

The first phenomenon of interest in this work is the escape of inner droplets as a consequence of the coalescence of the inner droplet with the external continuous phase, i.e. by drainage of the film between the inner droplet and the boundary of the outer droplet. Different approaches were proposed in the literature to model this phenomenon and will be investigated in detail in the modelling section. For instance, Pays et al. (2001) [21] assumed the escape rate to be proportional to a multiplication of two terms: the number of adsorbed inner droplets on the surface of the outer droplets and a coalescence frequency. They proposed an adsorption isotherm to predict the number of adsorbed inner droplets based on Fowler and Guggenheim model (1939) [22], while the escape (or coalescence) frequency was determined by fitting to experimental data. Klahn et al. (2002) considered the escape rate to be proportional to a

multiplication of three terms: the escape frequency, the escape probability and a critical region concerned by the escape phenomenon [23]. The escape frequency was determined from the circulation time on streamlines formed within an outer droplet present in a simple shear flow, the escape probability was obtained from the film drainage theory, while the fraction of the critical region was obtained by fitting to experimental data. Chávez-Páez et al. (2012) [16] conducted 3D simulations to describe the inner droplets Brownian motion and to estimate their collision frequency with the surface of outer droplet. The escape rate was then considered to be proportional to the collision frequency times a coalescence probability to be determined elsewhere. Kang et al. (2016) [24] considered that the droplets movement can be approximated by a Stokes flow. Based on this, they developed a model to calculate the dewetting time in double emulsions, or equivalently the escape time, based on momentum and energy conservation.

The second phenomena of interest in this work is droplets swelling. One of the earliest researches regarding the swelling phenomena in W/O/W double emulsions was performed by Matsumoto et al. [14,25–27]. By handling experiments in an optical microscope, the authors measured the swelling rate of W/O/W double emulsions and stated that it was not affected by the fraction of the inner droplets (ϕ_{μ}) (see Table 1). Their viscosity measurements of the double emulsions showed an increase with the osmotic pressure in the internal phase (which is controlled by the fraction of ions ϕ_{ions}) until a point above which it decreased. They calculated the permeability of different hydrocarbon oils using the membrane permeability model [26,28], but without including the effect of Laplace pressure (for inner droplets of 1-2 μm). They suggested that the physical state of the oil layer, its rheology, and so the permeation coefficient, is altered by the presence of ions [27]. Garti et al. (1985) [29] applied the same methodology to double emulsions undergoing shrinkage and estimated an increase in the permeability coefficient when increasing the fraction of the internal emulsifier ($\phi^{\mathrm{in}}_{\mathrm{emulsifier}}$) that was explained by possible micellar transport. The same phenomenon was observed by Yan and Pal (2001) [30] but they explained it by the diffusion of hydrated surfactant that may facilitate water transport. They also observed a slight decrease in the permeability when increasing the internal aqueous phase fraction (ϕ_{μ}) that was explained by a reduced free space for swelling.

Jager-Lezer (1997) found that increasing the lipophilic surfactant fraction ($\phi^{\text{in}}_{\text{emulsifier}}$) increased the swelling capacity and delayed the release. They indicated that increasing the amount of lipophilic emulsifier enhances the stability of the double emulsions while an excess would destabilize the emulsion [15]. These papers thus highlight opposing effects of the internal emulsifier on the swelling and release that are the increased viscosity, thus reducing permeability, and the diffusion of hydrated surfactant or potential micellar transport, thus increasing permeability. Similarly, a complex effect of the presence of ions on the rheology of the oil layer and the physical state of the surfactants is revealed. Besides the swelling capacity and permeation, a latent period was also pointed out in the literature. In a single drop-in-drop emulsion Bahtz et al. (2015) [31] investigated the initial stage of swelling and distinguished a lag period during which water migration was very slow. This lag period was found to be independent of the osmotic pressure gradient over the range of 2.7–13.3 bar and it was shorter for less viscous oil phases. For instance a lag period of ~10 min was found for an oil viscosity of 40 mPa.s. Jager-Lezer (1997) explained the latent period by the production of small inner droplets for which the Laplace counter pressure was higher, thus delaying the aqueous flow driven by the osmotic pressure gradient [15]. Table 1 summarizes the effects of the different parameters on the swelling rate and permeability.

From the literature review it appears that swelling is mainly studied as the direct effect of osmotic pressure gradient while the Laplace pressure was neglected, which can be justified only if the inner droplets are big. Consequently, the combined effect of the osmotic and Laplace pressures needs to be considered if smaller droplets are produced. Moreover, modeling both the swelling and the escape phenomena during storage were usually done by considering a mean inner and outer droplets size. However, in practice, double emulsions are polydisperse and using the mean diameter may fail to give the full understanding of the system. In order to allow for a thorough understanding of the double emulsion stability, it is required to consider the full droplet size distribution of both the inner and outer droplets by incorporating the individual models of the swelling and escape phenomena into population balance models (PBM) of both phases. In a previous work, we proposed a population balance model for the preparation step of double emulsions involving droplet breakage, coalescence and leakage

(using one PBM for the outer droplets) [32], and in the present work we will be interested in the storage period, involving droplet swelling and escape, where coupled inner and outer droplets PBMs are required.

The objective of this study is therefore to develop a coupled PBM for the inner and outer droplet size distributions (DSD) of W/O/W double emulsions undergoing droplet escape and swelling during storage. The escape and swelling models are developed respectively based on the dewetting model of Kang et al. (2016) [24] and the permeability model of membranes including the Laplace pressure effect. The release rate is monitored using conductivity and the evolution of the outer DSD using laser diffraction. The DSD of inner droplets is measured right after the first step of preparation using dynamic light scattering. A number of key operating parameters are varied: the internal water fraction, the stirring rate in the second preparation step, the salt fraction, and the fraction of the primary emulsion.

2. Experimental

The constituents used for double emulsion preparation are mineral oil (Fisher Scientific™), Span 80 (Alfa Aesar) as hydrophobic internal emulsifier, Tween 80 (Fisher Scientific™) as hydrophilic external emulsifier, sodium chloride as tracer and Millipore water (resistivity ≈ 18.2 $m\,\Omega\,.\,cm$).

Double emulsions were prepared in two steps. Table 2 shows the fractions used in the different experiments. In the first step, the NaCl solution was dispersed in the oil phase (composed of mineral oil and Span 80, typically at 0.314 mol L^{-1}, see Table 2) to produce the primary W/O emulsion using an IKA T 25 digital ULTRA-TURRAX® at 12 000 rpm for 4 min. In the second step, the primary emulsion was dispersed in an external aqueous phase (composed of water and Tween 80, at 0.0078 mol L^{-1}) to produce the W/O/W double emulsion. The second step was done in a 1-L stirred tank, equipped with four baffles, and stirring was done at 300-500 rpm for 70 min using a three-bladed stainless-steel impeller.

Right after the preparation of the primary emulsion, the DSD of the inner droplets was measured by using dynamic light scattering (Malvern Zetasizer Nano ZS®). The outer droplets

DSD was measured after the second step of preparation as well as during storage by means of Laser diffraction (Mastersizer 3000®).

A CDM210 Conductivity Meter (MeterLab®) was used to measure the conductivity of the samples, right after the second preparation step and during storage, in order to determine the released amount of encapsulated NaCl. A predetermined calibration curve was prepared either by dissolving different NaCl concentrations in O/W emulsion or in pure water. No effect of the oil was observed on the calibration curve in the studied concentration range, thus both methods were found equivalent.

3. Modeling

During storage, the inner (i.e. the micro-) droplets may undergo coalescence and swelling/shrinkage, or may escape. In the considered system, the inner salt concentration is higher than the outer concentration, and therefore the inner droplets would rather swell than shrink. The outer (i.e. the macro-) droplets may also undergo coalescence and swelling (due to inner droplets swelling) that may ultimately lead to breakdown due to overswelling. Since double emulsions are dilute and a high amount of stabilizer is used, the rate of coalescence was found to be negligible during storage. The objective of this work is thus to model swelling and escape until the onset of overswelling-breakdown. These phenomena need to be implemented in population balance models for both the inner and outer droplets [33,34]. The two PBMs are coupled and should be solved simultaneously.

3.1. Coupled population balance models

The PBM representing the evolution of the number density function of the inner droplets, n_{μ} (m^{-3}, i.e. per inner droplet size), undergoing only swelling and escape is:

$$\frac{\partial n_{\mu}(t,v_{\mu})}{\partial t} + \frac{\partial\left(\mathbb{S}_{\mu}(t,v_{\mu})n_{\mu}(t,v_{\mu})\right)}{\partial v_{\mu}} = \mathfrak{R}_{\mathrm{es},\mu}(t,v_{\mu}) \qquad 1$$

The PBM representing the evolution of the number density function of the outer droplets, n_{M} (m^{-3}, i.e. per outer droplet size) is:

$$\frac{\partial n_{\mathrm{M}}(t,v_{\mathrm{M}})}{\partial t}+\frac{\partial\left(\left[\mathbb{S}_{\mathrm{M}}(t,v_{\mathrm{M}})+Q_{\mathrm{es,M}}(t,v_{\mathrm{M}})\right]n_{\mathrm{M}}(t,v_{\mathrm{M}})\right)}{\partial v_{\mathrm{M}}}=0 \quad (2)$$

where v (m^3) is the droplets volume and the properties of the inner and outer droplets are indicated by the indices μ and M, respectively. The source term in eq. 1, $\Re_{\mathrm{es},\mu}$ (m^{-3} s^{-1}), represents the escape rate of inner droplets, which causes a change in the outer droplets volume represented by $Q_{\mathrm{es,M}}$ (m^3 s^{-1}). $\mathbb{S}_{\mu}$ (m^3 s^{-1}) is the volumetric swelling rate of the inner droplets that leads to swelling of the outer droplets, represented by $\mathbb{S}_{\mathrm{M}}$ (m^3 s^{-1}). The second terms on the lhs of equations 1 and 2 represent the growth/shrinkage of the inner and outer droplets respectively. The growth (i.e. when $\mathbb{S}_{\mu}>0$, $\mathbb{S}_{\mathrm{M}}>0$) or shrinkage (i.e. $\mathbb{S}_{\mu}<0$, $\mathbb{S}_{\mathrm{M}}<0$) are due to the osmotic pressure gradient which may lead to water diffusion in (i.e. swelling) or out (i.e. shrinkage) of the droplets. The escape of inner droplets may also cause shrinkage of the outer droplets. With only the growth/shrinkage term present in a population balance and a source terms equal to zero, the total number of droplets would be conserved and only their size may change. This is the case of the outer droplets which conserve a constant number, while the number of inner droplets reduces due to their escape. The models of droplets escape and swelling, required in the PBMs, are investigated in the following sections.

3.2. Swelling of inner and outer droplets

By analogy to Fick's law of diffusion and according to Starling's hypothesis, the net fluid flow through a membrane can be assumed to be proportional to the difference between the osmotic pressure gradient and the hydrostatic pressure [28,35]. Thus, swelling of the inner droplets is driven by the osmotic pressure gradient ($\Delta\Pi$) and it is countered by the Laplace pressure (ΔP) [15]. The Laplace pressure is commonly neglected when modelling swelling in the literature, but it will be accounted for in this work as the model will be applied to submicronic inner droplets where the Laplace pressure effect is not negligible. Considering the oil phase as an ideally selective membrane (i.e. permeable only to solvent), the volumetric swelling rate of an inner droplet, $\mathbb{S}_{\mu}$ (m^3 s^{-1}), can be written as follows:

$$\mathbb{S}_{\mu}(t,v_{\mu})=\frac{\mathrm{d}v_{\mu}}{\mathrm{d}t}=L_{\mathrm{p}}A_{\mu}(v_{\mu})\left(\Delta\Pi-\Delta P(v_{\mu})\right) \quad (3)$$

where L_p (m^2 s kg^{-1}) is the permeability coefficient of the membrane and A (m^2) the droplet's surface area. By this equation, when the osmotic pressure gradient is exactly counterbalanced by the Laplace pressure, equilibrium is reached and no mass transfer (swelling or shrinkage) occurs. The osmotic pressure gradient between the internal and external aqueous phases, $\Delta\Pi$ (Pa), is [36,37]:

$$\Delta\Pi = \Pi_{in} - \Pi_{out} = i\,R\,T\,(C_{in} - C_{out}) \quad (4)$$

Where i is the van't Hoff factor estimated to be 2 for NaCl [36], R (J K^{-1} mol^{-1}) the universal gas constant, T (K) temperature and C (mol m^{-3}) the concentration of salt (in and out stand for the inner and outer water phases, respectively). The Laplace pressure of inner droplets, ΔP (Pa), is:

$$\Delta P(v_\mu) = \frac{4\,\sigma_{\mu,M}}{d_\mu} \quad (5)$$

where d (m) is the droplets diameter and σ (N m^{-1}) the interfacial tension (here between inner and outer droplets).

As a consequence of inner droplets swelling, the volume of the outer droplets will increase. Considering the inner droplets to be initially evenly distributed among the outer droplets, the swelling rate of the outer droplets, $\mathbb{S}_M$ (m^3 s^{-1}), can be obtained by integrating the swelling rates of the encapsulated inner droplets:

$$\mathbb{S}_M(t, v_M) = \frac{dv_{M,swelling}}{dt} = \frac{v_M}{V_M(t)} \int_0^\infty n_\mu(t, v_\mu)\,\mathbb{S}_\mu(t, v_\mu)\,dv_\mu \quad (6)$$

where V_M is the total volume of the outer droplets. Equation 6 indicates for instance that increasing the number of inner droplets in an outer droplet would increase the swelling rate of the outer droplet.

Concerning the diffusion of water through the oil layer, two mechanisms were suggested in the literature. Garti et al. (1985) [29] explained water transfer based on micellar transport while Yan and Pal (2001) [30] explained it by the diffusion of hydrated surfactant that facilitates water transport.

It is also to be noted that in this model swelling of the outer droplets is totally governed by the swelling of the inner droplets. The literature regarding modeling of double emulsions did not

point out an effect of the outer interfacial tension on swelling (by opposing the osmotic pressure gradient). If such an effect is present, it would be lumped into the parameter L_{p} (the permeability coefficient of the membrane). This parameter includes the different molecular phenomena (e.g., effects of both surfactants, thickness/viscosity of the layer, etc.…) responsible for the resistance force.

3.2. Escape of inner droplets

Escape rate. The inner droplets may escape if they get close to the outer droplet surface. Different approaches were considered in the literature to model the escape rate (Table 3). Pays et al. (2001) assumed that the escape may only concern the inner droplets adsorbed on the surface of the outer droplets and they used an adsorption isotherm to evaluate the amount of adsorbed droplets [21]. In a simple shear flow, Klahn et al. (2002) considered that the escape may concern droplets present in a critical region close to the surface, of volume fraction α_{cr} [23]. In this case, the change in the number density of inner droplets n_{μ} with time is proportional to the change in their number in the critical region, with $n_{\mu}^{\mathrm{cr}} = \alpha_{\mathrm{cr}}\, n_{\mu}$. This concept can be assumed to be valid in general. The escape rate can therefore be written as, $\mathfrak{R}_{\mathrm{es},\mu}$(m^{-3} s^{-1}):

$$\mathfrak{R}_{\mathrm{es},\mu}(t, v_{\mu}) = -\alpha_{\mathrm{cr}}\, n_{\mu}(t, v_{\mu})\, \frac{1}{N_{\mathrm{M}}} \int_0^{\infty} \Omega_{\mathrm{es}}(v_{\mu}, v_M) n_{\mathrm{M}}(t, v_{\mathrm{M}})\, dv_{\mathrm{M}} \qquad 7$$

where N_{M} is the total number of outer droplets, $\Omega_{\mathrm{es}} = 1/t_{\mathrm{es}}(v_{\mu}, v_M)$ (s^{-1}) is the escape frequency with t_{es} (s) the escape time. From equation 7 it can be seen for instance that increasing the number of inner droplets would increase the escape frequency.

The overall escape rate of inner droplets from each outer droplet then causes a decrease in the volume of the outer droplet, $Q_{\mathrm{es,M}}$ (m^3 s^{-1}):

$$Q_{\mathrm{es,M}}(t, v_{\mathrm{M}}) = \frac{\mathrm{d}v_{\mathrm{M,escape}}}{\mathrm{d}t} = \frac{v_{\mathrm{M}}}{V_{\mathrm{M}}(t)} \int_0^{\infty} \mathfrak{R}_{\mathrm{es},\mu}(t, v_{\mu})\, v_{\mu}\, dv_{\mu} \qquad 8$$

Escape frequency. Klahn et al. [23] estimated the escape frequency of double emulsions undergoing a simple shear from the circulation time (Table 3). For emulsions under storage, droplets move only due to Brownian motion. In this case, Chávez-Páez et al. (2012) [16] considered the escape frequency to be governed by the collision frequency of inner droplets

with the surface of the outer droplet which is driven by their Brownian motion. They employed 3D simulations to calculate this frequency. Kang et al. (2016) proposed to calculate the escape time (inverse of the escape frequency) from the coalescence or dewetting time of inner droplets through the surface of the outer droplets [24,38]. This approach is applicable to double emulsions under storage and does not require heavy calculations compared to 3D simulations. The methodology is based on balancing the force caused by the interfacial tension and the viscous force. First, the escape time can be obtained by integrating the speed function over the crossed distance l (m) as follows:

$$t_{\mathrm{es}}(v_{\mu}, v_{M}) = \int_{0.01}^{L_{\mathrm{eq}}} \frac{1}{u_{\mu}(v_{\mu}) + u_{\mathrm{M}}(v_{\mathrm{M}})} dL \qquad 9$$

where u (m s^{-1}) is the velocity, $L = 2\ l/d_{\mu}$ a dimensionless position and L_{eq} the final position of the inner droplet at equilibrium, with $L_{\mathrm{eq}} = 2$ for complete separation/escape (i.e. when $l = d_{\mu}$). The lower bound of the integral corresponds to 0.5 % of d_{μ} considered as a threshold of dewetting.

The velocities are calculated based on momentum and energy conservations. If the viscosity of the continuous phase is small compared to the globules, the momentum conservation of the inner and outer droplets can be written as:

$$m_{\mu}\ u_{\mu}(v_{\mu}) = m_{\mathrm{M}}\ u_{\mathrm{M}}(v_{\mathrm{M}}) \qquad 10$$

where m (kg) is the droplet's mass.

During the dewetting phenomenon, on one hand, the driving force of separation (F_{S}) is governed by the interfacial tensions across the three phases: the inner droplet with outer droplet ($\sigma_{\mu,\mathrm{M}}$), the outer droplet with the outer continuous phase ($\sigma_{\mathrm{M,out}}$) and the inner droplet with the outer continuous phase ($\sigma_{\mu,\mathrm{out}}$, null in the present work). Kang et al. defined this force as [24]:

$$F_{\mathrm{S}}(v_{\mu}, v_{M}) = \pi\ d_{\mu}\ L(2 - L)\sigma_{\mu,\mathrm{M}}\left(1 - \frac{\sigma_{\mu,\mathrm{out}}}{\sigma_{\mu,\mathrm{M}}} + \frac{\sigma_{\mathrm{M,out}}}{\sigma_{\mu,\mathrm{M}}}\frac{1}{K}\right) \qquad 11$$

where $K = \frac{d_{\mathrm{M}}}{d_{\mu}}$.

On the other hand, the resistance force to escape (F_{V}) is governed by the viscosity of the outer droplet, as the viscosity of the continuous phase is negligible compared to the outer droplet. Kang et al. defined this force by:

$$F_{\mathrm{V}}(v_{\mu}, v_{\mathrm{M}}) = \frac{3}{2}\pi\, d_{\mu}\eta_{\mathrm{M}}\left[u_{\mu}(v_{\mu}) + u_{\mathrm{M}}(v_{\mathrm{M}})\right](2 - L) \quad (12)$$

The energy conservation implies:

$$\int_{0.01}^{L}\left[F_{\mathrm{S}}(v_{\mu}, v_{\mathrm{M}}) - F_{\mathrm{V}}(v_{\mu}, v_{\mathrm{M}})\right]dL = \frac{1}{2}m_{\mu}u_{\mu}^{2}(v_{\mu}) + \frac{1}{2}m_{\mathrm{M}}u_{\mathrm{M}}^{2}(v_{\mathrm{M}}) \quad (13)$$

The velocities are calculated by solving equations 10-13 analytically. This allows to calculate the dewetting time (eq. 9), and thus the escape frequency.

Fig. 1A shows the calculated escape frequency for different inner and outer droplets diameters. The escape frequency decreases for bigger outer droplets and in this case the size of the inner droplets has a negligible effect. For smaller outer droplets, the escape frequency is higher, and the impact of the size of the inner droplet is significant (bigger inner droplets lead to higher escape frequencies). Indeed, smaller inner droplets have a higher velocity. Fig. 1B shows that higher oil viscosities lead to much lower escape frequencies. Indeed, the viscosity has a great impact on the speed of the inner droplets.

3.3. Numerical solution

The semi-discrete finite volume scheme is adapted to solve a population balance involving a growth (or swelling) term, G ($m^3\ s^{-1}$) (Qamar and Warnecke 2007 [39], Kumar and Warnecke (2010) [40]). In the finite volume method, the PBM is reformulated into a mass balance, $g(t, v) = v\, n(t, v)$. By discretizing the flux across the cell boundaries $[i + \frac{1}{2}, i - \frac{1}{2}]$ and setting $\tilde{G} = \frac{G}{v}$, one obtains:

$$\frac{dg_i(t,v)}{dt} = -\frac{v_i}{\Delta v_i}\left[\left(\tilde{G}\, g\right)_{i+\frac{1}{2}} - \left(\tilde{G}\, g\right)_{i-\frac{1}{2}}\right] \quad (14)$$

with:

$$\left(\tilde{G}\, g\right)_{i+\frac{1}{2}} = \tilde{G}_{i+\frac{1}{2}}\left[g_i + \frac{\Delta v_i}{2\Delta v_{i-\frac{1}{2}}}\,\Phi(r_i^{+})\,(g_{i+1} - g_i)\right] \quad (15)$$

in which $\Phi(r_i^+) = \frac{|r_i^+| + r_i^+}{1 + |r_i^+|}$ is the flux limiting function with $r_i^+ = \frac{g_i - g_{i-1} + \epsilon}{g_{i+1} - g_i + \epsilon}$ and the parameter ϵ is a small number used to avoid the division by zero [40,41].

4. Results and discussions

The developed models for inner droplets escape and swelling were incorporated into the PBMs of the inner and outer droplets and solved simultaneously using the semi-discrete finite volume numerical scheme [40]. The evolution of the release rate and the size distribution of the outer droplets were monitored during storage of the double emulsions. Different parameters were varied to evaluate the robustness of the combined models, including the fraction of the primary emulsion, the fraction of salt, the fraction of the internal phase and the effect of the stirring rate in the second step of preparation through its effect on the outer droplets size and the encapsulation efficiency (Table 2).

4.1 Observation of the swelling and escape phenomena

Few microscopic images of double emulsions are shown in Fig. 2 at different storage times. At day 0, right after the preparation, inner droplets (of 800 nm in diameter, as measured by the NanoZS) clearly appear to be encapsulated within the outer droplets (mean diameter of 40 µm). This image qualitatively confirms that the inner droplets size did not sensibly evolve during the second preparation step neither through inner-inner droplet coalescence nor swelling. After 6 days, both the inner and outer droplets have bigger sizes than initially, revealing either swelling or coalescence of these droplets during storage. After 20 days, the outer droplets have a smaller size than day 0, and many outer droplets appear to be almost empty from the inner droplets. This last observation clearly reveals an overswelling-breakdown phenomenon.

In order to investigate if cause of outer droplet growth (observed at day 6, Fig. 2) is due to droplets swelling or coalescence, a single O/W emulsion was prepared using the same oil phase (i.e. mineral oil + Span 80) without salt and stored under similar conditions as the double emulsion. Note that it is hard to produce a single emulsion that has exactly the same properties of the double emulsion in terms of size, viscosities, densities and surface tension. However, the

oil fraction ($\phi_{\text{oil+Span 80}} = 1$ %) was equivalent to the primary emulsion fraction in the double emulsion (ϕ_{M}) and similar external emulsifier concentrations ($\phi^{\text{out}}_{\text{emulsifier}} = 1$ %), stirring rate (ω_{R} = 400 rpm) and duration were employed. Under these conditions, the obtained mean droplets size distribution right after the preparation of the single emulsion (Fig. 3A) was comparable to the outer droplets size in the double emulsion (Fig. 3B). So, the single and double emulsions may be assumed to undergo similar coalescence rates. However, Fig. 3A shows that the single emulsion undergoes only slight coalescence during 19 days of storage while Fig. 3B shows that the size of the outer droplets in the double emulsion increases importantly during the first week, which is in agreement with the microscopic images (Fig. 2). It can thus be deduced that the observed growth of the outer droplets in the case of the double emulsion is mainly due to swelling caused by the osmotic pressure gradient, which is a well-known phenomenon in double emulsions containing ions [14,15,25,26,30,31].

The maximum swelling was found to occur after around one week of storage (6-8 days) for most samples, after which the double emulsions endured overswelling-breakdown (Fig. 2C and Fig3B). Thus, the predictions of swelling and release are done over one week in the following sections.

4.2. Parameter identification

Two model parameters need to be identified for the present system: the volume fraction of the critical region, α_{cr}, and the permeability coefficient, L_{P}. Three experiments were chosen among the experiments presented in Table 2 for parameter identification. The selected experiments were all prepared at 400 rpm stirring rate but they have different compositions: a) $\phi_{\text{M}} = 4$ %, $\phi_{\text{NaCl}} = 0.05$ %, $\phi_{\mu} = 40$ %; b) $\phi_{\text{M}} = 1$ %, $\phi_{\text{NaCl}} = 0.24$ %, $\phi_{\mu} = 40$ %; and c) $\phi_{\text{M}} = 1$ %, $\phi_{\text{NaCl}} = 0.05$ %, $\phi_{\mu} = 40$ %. The "MultiStart class" global optimization function of MATLAB® was used while employing "fmincon" nonlinear solver to perform the identification.

The identified parameters are given in Table 4. The identified permeability coefficient, L_{p}, is compared to the literature values and it can be seen that it is of the same order of magnitude. The permeability coefficient was found in the literature to depend on the oil viscosity and the fraction of internal emulsifier [15,25,26,29,30]. In this work, the oil type and the emulsifier

concentration were maintained the same in all experiments. Therefore, it was possible to fit a unique value of L_{P} for the three experiments used for the identification, $L_{\mathrm{p}} = 2.75 \times 10^{-15}$. This value, as well as the identified value of the critical region, $\alpha_{\mathrm{cr}} = 3.6 \times 10^{-5}$, will be kept constant in the model to predict the evolution of the other experiments. It is worthy to note however that the viscosity of the outer droplet evolves with time, due to swelling and release, which may lead to an evolution of the permeability, but this effect was not modelled.

Concerning the critical fraction α_{cr}, Klahn et al. [23] estimated a decrease in α_{cr} when increasing d_{M}/d_{μ}, (for instance, $\alpha_{\mathrm{cr}} = 0.2$ for $d_{\mathrm{M}}/d_{\mu} = 10$). However, their operating conditions and modelling approach favors the estimation of higher critical fractions than the present work ($\alpha_{\mathrm{cr}} = 3.6 \times 10^{-5}$). First of all, they applied a simple shear flow to the double emulsions, while in our case the double emulsions were stored under stagnant conditions. Second, in our case $d_{\mathrm{M}}/d_{\mu} \approx 50$, which should lead to lower fractions. Finally, they calculated the escape probability to be $P \approx 0.06$ while in our work P is regrouped with α_{cr} as in Pays et al. (i.e. $P = 1$). In the work of Pays et al. [21], the fraction of the adsorbed droplets (here regarded as α_{cr}) was not indicated, but it could be estimated to be around $\alpha_{\mathrm{cr}} = n_{\mu}^{cr}/n_{\mu} = 0.57$ (see Table 3). This is reasonable as in their study the escape was faster and the outer droplet was empty from inner droplets within 20 hours. Chávez-Páez et al. (2012) [16] simulated full escape in 1 second when employing an arbitrary escape probability of $P = 1 \times 10^{-3}$ and indicated that real probabilities should be lower.

4.3. Effect of the primary emulsion fraction (ϕ_M)

The effect of the primary emulsion fraction was investigated over the range of ϕ_{M} = 1 %, 2 %, 3 % and 4 % (set 1 in Table 2). Fig. 4 shows the model predictions compared to the experimental results for one of the experiments (with ϕ_{M} = 4 %), regarding the outer DSD (Fig. 4A) and the released fraction of NaCl (Fig. 4B). It can be seen that the model predictions are in good agreement with the experimental results for both variables. In this experiment, the encapsulation efficiency measured right after preparation was 95.5 % (Table 2). The plotted released fraction represents the amount released during storage only. To have the cumulative released fraction one needs to add the fraction released initially during preparation. For

instance in this experiment, after seven days, we obtain a released fraction of 28 % during storage alone and a cumulative released fraction of 31.24 %.

Fig. 5 shows the evolution of the outer and inner DSD and the escape rate during storage of the experiments in set 1, where the volume fraction of the primary emulsion ϕ_{M} was varied. As the initial DSDs are similar in all the experiments of this set, only one initial DSD is depicted on the figure for both the inner and outer droplets. The theoretical concentration of salt is the same in all the experiments of this set, but a slightly higher encapsulation efficiency was obtained when increasing ϕ_{M} ($EE = 92.5 - 95.5$ %), which is in line with the results reported by Matsumoto et al. [5]. As the differences in the encapsulation efficiencies are small, the experiments are comparable in terms of osmotic pressure gradients (which represents the driving force for swelling), and therefore they undergo similar swelling rates. A slightly higher swelling is observed in the inner DSD when increasing ϕ_{M} (Fig. 5B). Note that the inner droplets size changes only due to swelling and is not affect by the escape phenomenon. Concerning the outer DSD (Fig. 5A), it changes as a consequence of both swelling, as a primary factor, and escape, but at a much lower extent. In Fig. 4C, it can be seen that a slightly lower escape rate is observed for higher primary fractions ϕ_{M}. As a global result, the measured outer DSDs are similar for the different fractions.

Fig. 5B shows that the DSD of inner droplets gets deformed with time and deviates from its initial Gaussian distribution. This is explained by the fact that the swelling rate is governed by $\mathbb{S}_{\mu}(t, v_{\mu}) \propto \left[\Delta\Pi - \Delta P(v_{\mu})\right]$. Therefore, within the droplets of the distribution, smaller droplets have a higher Laplace pressure, and may attain $\Delta P \geq \Delta\Pi$, and consequently stop swelling before bigger droplets. As a consequence, only a very small number of the inner droplets continues to swell to the size of about 10 µm (estimated by the model to be less than 5 % in number in all experiments). Quantitative measurement of the inner droplet's size distribution represents a big challenge [19], but a qualitative confirmation could be obtained by microscopy. This simulation shows the advantage compared to models neglecting the Laplace pressure. Indeed, if the Laplace pressure is neglected, all the droplets would continue to swell until reaching osmotic equilibrium ($\Delta\Pi = 0$), as no other force would oppose swelling.

4.4. Effect of the salt fraction (ϕ_{NaCl})

The ions fraction controls the osmotic pressure gradient, which represents the driving force for swelling. In this section, the effect of this key parameter is investigated over the range of ϕ_{NaCl} = 0.05 %, 0.14 %, 0.19 % and 0.24 % (set 2 in Table 2). The encapsulation efficiency was found to slightly increase when increasing the salt fraction: $EE = 92.5 - 96.4$ %. Note that the change in the salt fraction led to a change in the measured interfacial tension from 4 mN.m^{-1} to 5 mN.m^{-1}, respectively. Such change was not found to importantly impact the calculation and therefore a constant value of 5 mN.m^{-1} was implemented.

Fig. 6A shows the inner DSD measured after the preparation of the first emulsion for the different experiments in the set. It can be seen that the inner droplets size increases when increasing the salt fraction over the range of $\phi_{\mathrm{NaCl}} = 0.05 - 0.19$ %, but much smaller sizes are obtained with the highest salt fraction ($\phi_{\mathrm{NaCl}} = 0.24$ %). It is known that the ions may affect the surfactant spreading and oil viscosity leading to a complex effect on the stability during preparation, which may lead to this optimal point [8,32,42]. During storage (Fig. 6B), the model predicts that the swelling of the inner droplets increases when increasing the salt fraction. As the experiment with $\phi_{\mathrm{NaCl}} = 0.24$ % had initially the smallest droplets size, it remained smaller than two experiments with higher salt fractions ($\phi_{\mathrm{NaCl}} = 0.14$ and 0.19 %) but exceeded the size of the experiment with $\phi_{\mathrm{NaCl}} = 0.05$ %.

Concerning the outer droplets, Fig. 6C shows that the model predictions of the outer DSD after one week are in good agreement with the experimental measurements for all salt concentrations. Besides, it can be seen that increasing the salt fraction has a negligible effect on the outer DSD when the salt fraction is high ($\phi_{\mathrm{NaCl}} \geq 0.14$ %). Indeed, the double emulsions in the different experiments seem to swell up to a maximum swelling capacity where the fraction of salt has no effect. With a lower salt fraction ($\phi_{\mathrm{NaCl}} = 0.05$ %), the droplets swell to much smaller sizes after one week, which can be due to a lower inner droplets swelling rate combined to higher inner droplets escape. Indeed, for the experiment with $\phi_{\mathrm{NaCl}} = 0.05$ % the release was approximately 40 % after one week (see experiment $\phi_{\mathrm{M}} = 1$ % in Fig. 5C) while a negligible fraction was released in the experiments with high salt fractions ($\phi_{\mathrm{NaCl}} \geq 0.14$ %).

The difference in the escape rates can be explained by the differences in the size of the inner droplets, as explained in Fig. 1 (bigger inner droplets lead to a higher escape frequency). A higher escape rate contributes to a reduction in the osmotic pressure gradient with time, which leads to less swelling. This is in line with the literature, where a higher swelling rate was observed for higher osmotic pressure gradients [25,30,31]. Moreover, Jager-Lezer (1997) reported in general a lower release for higher swelling [15], as observed here.

It is to be noted that in the employed model the salt fraction affects the escape rate indirectly through its effect on the size. Indeed, the salt fraction is not considered in the dewetting model proposed by Kang et al. (2016) [24]. It might be considered that the salt has a direct effect on the escape rate through its influence on the surface or viscosity forces [43]. This would require to account for the complex effects of salt on the surfactant and rheological behavior of the double emulsion. In the present work, the proposed model fits well the experimental data and has the advantage of being simple to implement. But, the identified parameters would be inaccurate if some phenomena are neglected.

4.5. Effect of the internal phase fraction (ϕ_μ)

The internal phase was varied over the range of $\phi_\mu = 10$ %, 20 %, 30 % and 40 % (set 3 in Table 2). The amount of salt was maintained constant and only the fraction of water to oil was varied. Therefore, when increasing ϕ_μ, the osmotic pressure gradient between the inner and outer water theoretically decreases. The encapsulation efficiency was found to importantly increase when increasing ϕ_μ: $EE = 51.2 - 92.5$ %. As a result, the real osmotic pressure gradient remained lower when increasing ϕ_μ. The increase in the encapsulation efficiency with ϕ_μ can be explained by an increased viscosity of the outer droplets, following the viscosity model of Vermeulen (1955) [44]. A higher apparent viscosity leads to a decrease in the escape rate during preparation. Indeed, the escape rate during preparation is mainly due to leakage of the inner droplets during the breakage of the outer droplets [18,32,45]. The higher the internal phase fraction, the higher the viscosity of the outer droplets, which leads to a reduced breakage rate [46] and to a higher encapsulation efficiency [32]. Fig. 7A shows the initial DSD of the outer droplets measured just after preparation for the different experiments of this set. A

slight increase in the outer droplets size is observed when increasing ϕ_μ, which confirms the reduction in the breakage and therefore the leakage rate.

Fig. 7B shows the predictions of the evolution of the inner DSD after one week of storage. A slightly higher swelling is observed for the emulsions with lower ϕ_μ, which can be explained by the higher osmotic pressure gradient. Yan and Pal (2001) [30] also observed a slight decrease in droplets swelling for higher ϕ_μ up to 40 %, beyond which they observed a sharper decrease. Bahtz et al. [31] observed a negligible effect on the swelling rate when increasing ϕ_μ up to 30 %.

Fig. 7C shows the evolution of the outer DSD during storage, experimentally and by the model. It can be seen that increasing ϕ_μ leads to a very slight increase in the outer droplets size, which is partly due to their different initial sizes (Fig. 7A). Concerning the released fraction, it was approximately 40% for the experiment with $\phi_\mu = 40$ % (Fig. 5C), and around 15 % for the other experiments after one week of storage. This is in line with previous investigations where higher swelling rates imply lower release rates [15].

4.6. Effect of the stirring rate

Changing the stirring rate during the preparation of the double emulsion has a direct effect on the outer droplets size and the encapsulation efficiency, which may affect droplets swelling and escape during storage. The stirring rate was varied over the range of 300, 350, 400 and 500 rpm (set 4 in Table 2) leading respectively to mean Sauter diameters of d_{32} =29.4, 26, 24.5 and 24 µm and encapsulation efficiencies of 94.1 %, 93.3 %, 92.5 % and 88.1 %. It is known that a higher stirring leads to more breakage which causes more leakage of the inner droplets and therefore to a lower encapsulation efficiency [32]. Fig. 8A shows the DSD of the outer droplets measured right after preparation. As expected, smaller droplets are produced when increasing the stirring rate.

The internal emulsion was prepared under the same conditions in all the experiments of this set, and therefore only one initial experimental DSD is shown on Fig. 8B. The figure also shows the predictions of the swelling effect on the size of the inner droplets during storage which appears to be identical for all experiments. The size distribution of the outer droplets of the

different experiments of this set after one week of storage are shown in Fig. 8C The experiments conserve the same order of size as initially (Fig 8A)., where the biggest droplets measured after one week correspond to the experiment done with the lowest stirring rate. The released fraction after one week in all the experiments was found to be around 40%, which is due to the fact that the inner sizes and salt fractions are identical.

4.7. Evolution of the pressure gradients with time

The Laplace pressure counterbalances the osmotic pressure and should be overcome to lead the droplets to swell. Fig. 9A shows the evolution of the osmotic pressure gradient at different time steps and the Laplace pressure as a function of the size of the inner droplets. There is only one curve for the Laplace pressure as it depends on the droplet size and the surface tension which is assumed not to change with time. In contrast, the osmotic pressure decreases with time due to droplets swelling and therefore a selection of few time steps was made and plotted in the figure. The osmotic pressure is independent of the droplet size. The swelling is conditioned by $\Delta\Pi > \Delta P(v_{\mu})$, and only the fraction of droplets that have their sizes in the region where the osmotic pressure is higher than the Laplace pressure would swell. The critical size of the inner droplets corresponding to the intersection between $\Delta\Pi$ and ΔP becomes bigger with time, because $\Delta\Pi$ decreases due to swelling (that decreases C_{in}) and due to the escape (that slightly increases C_{out}).

Fig. 9B shows the swelling rates at the selected time steps as a function of the inner droplets size. The curves were forced to go to zero in the region of sizes where no droplets exist or when $\Delta\Pi \leq \Delta P(v_{\mu})$. As the swelling rate is $\mathbb{S}_{\mu}(t, v_{\mu}) \propto [\Delta\Pi - \Delta P(v_{\mu})]$, it increases when the difference between the osmotic and Laplace pressures increases. As $\Delta P(v_{\mu})$ decreases with the droplet size, a global increase in the swelling rate is observed over the size. Finally, the curves move towards bigger sizes with time, due to the creation of bigger droplets and the disappearance of small ones by swelling, besides the fact that some small droplets stop to swell when $\Delta\Pi \leq \Delta P(v_{\mu})$.

Fig. 9C shows the evolution of the inner DSD at different times. The swelling phenomenon clearly leads to an increase in the size of the inner droplets. The change in the form of the

distribution from normal to bimodal is due to the fact that part of the droplets become smaller than the critical size bellow which no swelling occurs. In fact only a small number fraction of the inner droplets (here 2.67 %) is estimated to continue to swell up to 5-10 μm.

Fig. 9D shows the DSD of the outer droplets at the different times. The outer droplets quickly attain a big size and only undergo a little change afterwards. This is due to the fact that the main part of the inner droplets stop swelling when the osmotic pressure gradient is counterbalanced by the Laplace pressure. The model is fitting the experimental data very well at day six, but there is a slight difference at day one. This may be due to an evolution of the permeation coefficient with time, due to swelling and escape, which affect for instance the rheology of the double emulsion. This difference is in line with the swelling lag time reported in the literature, for instance by Bahtz et al. (2015) [31], that is not accounted for by the model. Indeed, it is preferable to have a unique permeation coefficient with time, as estimating different values would make the model empirical. The evolution in the rheology should be described by a fundamental model and allow an automatic evolution of the permeation coefficient, which may constitute an improvement of this model.

5. Conclusions

The escape and swelling rates of the inner droplets and the swelling of the outer droplets were incorporated into the population balances of the inner and outer droplets in order to predict the evolution of the droplets size and the release rate during storage of double emulsions. The PBMs allow the prediction of the full size distribution of the droplets. The Laplace pressure gradient was accounted for in the swelling model. The model parameters were identified and validated for a wide range of operating conditions.

It was found that the main growth of the outer droplets during storage is due to the swelling of the inner droplets, due to osmotic pressure gradient. The extent of coalescence was found negligible, and the effect of inner droplets escape on the outer droplets diameter is minor compared to the swelling effect. The effect of the Laplace pressure is essential and leads to stopping the swelling of the inner droplets before osmotic equilibrium.

The two models were found to give good predictions over a wide range of conditions. The change in the fraction of the primary phase (1–4%) was found to cause a slight increase in the inner droplets swelling and a slightly lower escape rate, while almost no effect could be observed on the outer droplets. Increasing the salt fraction was found to have a complex effect on the inner droplets size during preparation and led to a higher swelling rate and lower escape during storage. Increasing the internal phase fraction led to bigger outer droplets due to their higher apparent viscosities, and during storage the DSD showed a slight increase in the inner droplets swelling due to the higher ions fraction. Higher stirring rates led to smaller outer droplets but no effect was observed on the swelling rate. Most emulsions seem to reach a kind of maximum size during swelling. This could be explained by the fact that most of the inner droplets stop swelling when the osmotic pressure gradient decreases, mainly due to swelling, which becomes compensated by the Laplace pressure.

The developed model still needs to be evaluated on a wider range of operating conditions, mainly for different inner and outer surfactant types and different oils (with different viscosities, densities, interfacial tension, etc.). This work has put the basis of the coupled PBMs of inner and outer droplets to describe the stability of double emulsions during storage that should be able incorporate new parameters straightforwardly.

Acknowledgement

This work was funded by ModLife ITN. Grant agreement number 675251.

Nomenclature

A surface area of the droplet [m^2]

A_H Hamaker constant [J] (Table 3)

C salt concentration [mol m^{-3}]

d diameter of the droplet [m]

D_i diffusion coefficient of particle i [m^2 s^{-1}] (Table 3)

F_i total force acting on particle i [N] (Table 3)

F_{S} driving force of separation [N]

F_{V} resistance force to escape [N]

g size distribution in volume density [$m^3\ m^{-3}$]

G growth or shrinkage [$m^3\ s^{-1}$]

i van't Hoff factor [-]

K ratio of the outer to inner droplet diameter, $K = \frac{d_{\mathrm{M}}}{d_{\mu}}$, [-]

$\mathrm{k_B}$ Boltzman constant [$m^2\ kg\ s^{-2}\ K^{-1}$]

l inner droplet crossed distance [m]

l_{s} average length of surface tails [m] (Table 3)

L dimensionless position [-]

L_{ij} distance between particles i and j [m] (Table 3)

L_{p} permeability coefficient of membrane [$m^2\ s\ kg^{-1}$]

m mass of the droplet [kg]

n number density [m^{-3}, i.e. per droplet's size]

n_0 total number density of available sites for adsorption (Table 3)

N_{M} total number of the droplets

P escape probability [-]

P_0 permeation coefficient [$m\ s^{-1}$]

$Q_{\mathrm{es,M}}$ rate of change in outer droplets volume due to escape of inner droplets [$m^3\ s^{-1}$]

r_i position [m] (Table 3)

r_i^+ upwind ratio of two consecutive solution gradients [-]

R universal gas constant [$J\ K^{-1}\ mol^{-1}$]

R_i random displacement [m] (Table 3)

$\mathfrak{R}_{\mathrm{es},\mu}$ escape rate of inner droplets [m^{-3} s^{-1}]

$\mathbb{S}$ swelling rate [m^3 s^{-1}]

t time [s]

T temperature [K]

u velocity of the droplet [m s^{-1}]

u_{a} adsorption energy [J] (Table 3)

u_{l} latent energy of interaction between droplets [J] (Table 3)

v volume of the droplet [m^3]

V total volume of the droplets [m^3]

V_{w}^{*} molar volume of pure water [m^3 mol^{-1}]

z screening constant [-] (Table 3)

Greek letters

α_{cr} volume fraction of the critical region of escape [-]

$\dot{\gamma}$ shear rate [s^{-1}] (Table 3)

ΔP Laplace pressure [Pa]

ε dimensionless energy parameter [-] (Table 3)

ϵ a small number (e.g., $\epsilon = 10^{-10}$) to avoid the division by zero

η viscosity [Pa s]

Θ fraction of occupied sites [-] (Table 3)

Π osmotic pressure [Pa]

σ interfacial tension [N m^{-1}]

τ time spent by an inner droplet on the surface of the outer droplet [s] (Table 3)

Φ flux limiting function [-]

Ω_{es} escape frequency [s^{-1}]

Subscripts

c circulation (Table 3)

d drainage (Table 3)

eq equilibrium

es escape

i interaction (Table 3)

in inner phase

M outer (or Macro-) droplet

out outer (external) phase

μ inner (or micro-) droplet

References

[1] G. Muschiolik, Multiple emulsions for food use, Current Opinion in Colloid & Interface Science. 12 (2007) 213–220. doi:10.1016/j.cocis.2007.07.006.

[2] A. Aserin, ed., Multiple emulsions: technology and applications, Wiley-Interscience, Hoboken, N.J, 2008.

[3] W.S.W. Ho, K.K. Sirkar, eds., Membrane Handbook, Springer US, Boston, MA, 1992. doi:10.1007/978-1-4615-3548-5.

[4] W. Seifriz, Studies in Emulsions. I-II, The Journal of Physical Chemistry. 29 (1924) 587–600. doi:10.1021/j150251a008.

[5] S. Matsumoto, Y. Kita, D. Yonezawa, An attempt at preparing water-in-oil-in-water multiple-phase emulsions, Journal of Colloid and Interface Science. 57 (1976) 353–361. doi:10.1016/0021-9797(76)90210-1.

[6] A. Schuch, J. Wrenger, H.P. Schuchmann, Production of W/O/W double emulsions. Part II: Influence of emulsification device on release of water by coalescence, Colloids and Surfaces A: Physicochemical and Engineering Aspects. 461 (2014) 344–351. doi:10.1016/j.colsurfa.2013.11.044.

[7] T. Schmidts, D. Dobler, C. Nissing, F. Runkel, Influence of hydrophilic surfactants on the properties of multiple W/O/W emulsions, Journal of Colloid and Interface Science. 338 (2009) 184–192. doi:10.1016/j.jcis.2009.06.033.

[8] T. Schmidts, D. Dobler, P. Schlupp, C. Nissing, H. Garn, F. Runkel, Development of multiple W/O/W emulsions as dermal carrier system for oligonucleotides: Effect of additives on

emulsion stability, International Journal of Pharmaceutics. 398 (2010) 107–113. doi:10.1016/j.ijpharm.2010.07.037.
[9] M. Frenkel, R. Shwartz, N. Garti, Multiple emulsions, Journal of Colloid and Interface Science. 94 (1983) 174–178. doi:10.1016/0021-9797(83)90247-3.
[10] L. Zeng, Y. Zhang, C. Bukirwa, W. Li, Y. Yang, Study of mean diameter and drop size distribution of emulsion drops in a modified rotating disc contactor for an emulsion liquid membrane system, RSC Advances. 5 (2015) 89959–89970. doi:10.1039/C5RA16267J.
[11] J. Yan, R. Pal, Isotonic swelling behavior of W/O/W emulsion liquid membranes under agitation conditions, Journal of Membrane Science. 213 (2003) 1–12. doi:10.1016/S0376-7388(02)00501-X.
[12] R.M. Pfeiffer, A.L. Bunge, W. Navidi, Leakage and Swell in Emulsion Liquid-Membrane Systems: Batch Experiments, Separation Science and Technology. 38 (2003) 519–539. doi:10.1081/SS-120016649.
[13] S. Mukhopadhyay, S.K. Ghosh, V.A. Juvekar, Mathematical model for swelling in a liquid emulsion membrane system, Desalination. 232 (2008) 110–127. doi:10.1016/j.desal.2008.01.009.
[14] S. Mataumoto, W.W. Kang, FORMATION AND APPLICATIONS OF MULTIPLE EMULSIONS, Journal of Dispersion Science and Technology. 10 (1989) 455–482. doi:10.1080/01932698908943184.
[15] N. Jager-Lezer, I. Terrisse, F. Bruneau, S. Tokgoz, L. Ferreira, D. Clausse, M. Seiller, J.-L. Grossiord, Influence of lipophilic surfactant on the release kinetics of water-soluble molecules entrapped in a W/O/W multiple emulsion, Journal of Controlled Release. 45 (1997) 1–13. doi:10.1016/S0168-3659(96)01507-6.
[16] M. Chávez-Páez, C.M. Quezada, L. Ibarra-Bracamontes, H.O. González-Ochoa, J.L. Arauz-Lara, Coalescence in Double Emulsions, Langmuir. 28 (2012) 5934–5939. doi:10.1021/la205144g.
[17] R. Mezzenga, B.M. Folmer, E. Hughes, Design of Double Emulsions by Osmotic Pressure Tailoring, Langmuir. 20 (2004) 3574–3582. doi:10.1021/la036396k.
[18] A.J. Shere, H.M. Cheung, MODELING OF LEAKAGE IN LIQUID SURFACTANT MEMBRANE SYSTEMS, Chemical Engineering Communications. 68 (1988) 143–164. doi:10.1080/00986448808940403.
[19] F. Wolf, L. Hecht, H.P. Schuchmann, E.H. Hardy, G. Guthausen, Preparation of $W_1/O/W_2$ emulsions and droplet size distribution measurements by pulsed-field gradient nuclear magnetic resonance (PFG-NMR) technique, European Journal of Lipid Science and Technology. 111 (2009) 730–742. doi:10.1002/ejlt.200800272.
[20] A.. Florence, D. Whitehill, Some features of breakdown in water-in-oil-in-water multiple emulsions, Journal of Colloid and Interface Science. 79 (1981) 243–256. doi:10.1016/0021-9797(81)90066-7.
[21] K. Pays, J. Giermanska-Kahn, B. Pouligny, J. Bibette, F. Leal-Calderon, Coalescence in Surfactant-Stabilized Double Emulsions, Langmuir. 17 (2001) 7758–7769. doi:10.1021/la010735x.
[22] S.R. Fowler, E.A. Guggenheim, Statistical thermodynamics, University Press: Cambridge, 1939.

[23] J.. Klahn, J.J.. Janssen, G.E.. Vaessen, R. de Swart, W.G.. Agterof, On the escape process during phase inversion of an emulsion, Colloids and Surfaces A: Physicochemical and Engineering Aspects. 210 (2002) 167–181. doi:10.1016/S0927-7757(02)00376-X.
[24] Z. Kang, P. Zhu, T. Kong, L. Wang, A Dewetting Model for Double-Emulsion Droplets, Micromachines. 7 (2016) 196. doi:10.3390/mi7110196.
[25] S. Matsumoto, M. Kohda, The viscosity of W/O/W emulsions: an attempt to estimate the water permeation coefficient of the oil layer from the viscosity changes in diluted systems on aging under osmotic pressure gradients, Journal of Colloid and Interface Science. 73 (1980) 13–20.
[26] S. Matsumoto, T. Inoue, M. Kohda, K. Ikura, Water permeability of oil layers in W/O/W emulsions under osmotic pressure gradients, Journal of Colloid and Interface Science. 77 (1980) 555–563.
[27] S. Matsumoto, P. Sherman, A PRELIMINARY STUDY OF W/O/W EMULSIONS WITH A VIEW TO POSSIBLE FOOD APPLICATIONS, Journal of Texture Studies. 12 (1981) 243–257. doi:10.1111/j.1745-4603.1981.tb01234.x.
[28] O. Kedem, A. Katchalsky, Thermodynamic analysis of the permeability of biological membranes to non-electrolytes, Biochimica et Biophysica Acta. 27 (1958) 229–246.
[29] N. Garti, S. Magdassi, D. Whitehill, Transfer phenomena across the oil phase in water-oil-water multiple emulsions evaluated by Coulter counter: 1. Effect of emulsifier 1 on water permeability, Journal of Colloid and Interface Science. 104 (1985) 587–591.
[30] J. Yan, R. Pal, Osmotic swelling behavior of globules of W/O/W emulsion liquid membranes, Journal of Membrane Science. 190 (2001) 79–91.
[31] J. Bahtz, D.Z. Gunes, E. Hughes, L. Pokorny, F. Riesch, A. Syrbe, P. Fischer, E.J. Windhab, Decoupling of Mass Transport Mechanisms in the Stagewise Swelling of Multiple Emulsions, Langmuir. 31 (2015) 5265–5273. doi:10.1021/acs.langmuir.5b01138.
[32] B. Khadem, N. Sheibat-Othman, Modeling of double emulsions using population balance equations, Chemical Engineering Journal. 366 (2019) 587–597. doi:10.1016/j.cej.2019.02.092.
[33] D. Ramkrishna, A.W. Mahoney, Population balance modeling. Promise for the future, Chemical Engineering Science. 57 (2002) 595–606. doi:10.1016/S0009-2509(01)00386-4.
[34] D. Ramkrishna, Population balances: theory and applications to particulate systems in engineering, Academic Press, San Diego, CA, 2000.
[35] J.R. Pappenheimer, Passage of molecules through capillary walls, Physiological Reviews. 33 (1953) 387–423.
[36] O. Karnland, Bentonite swelling pressure in strong NaCl solutions. Correlation between model calculations and experimentally determined data, Swedish Nuclear Fuel and Waste Management Co., 1997.
[37] T.S.H. Leong, M. Zhou, N. Kukan, M. Ashokkumar, G.J.O. Martin, Preparation of water-in-oil-in-water emulsions by low frequency ultrasound using skim milk and sunflower oil, Food Hydrocolloids. 63 (2017) 685–695. doi:10.1016/j.foodhyd.2016.10.017.
[38] B. Khadem, N. Sheibat-Othman, Modeling stability of double emulsions, in: Computer Aided Chemical Engineering, Elsevier, 2017: pp. 493–498.

[39] S. Qamar, G. Warnecke, Numerical solution of population balance equations for nucleation, growth and aggregation processes, Computers & Chemical Engineering. 31 (2007) 1576–1589.
[40] J. Kumar, G. Warnecke, A note on moment preservation of finite volume schemes for solving growth and aggregation population balance equations, SIAM Journal on Scientific Computing. 32 (2010) 703–713.
[41] B. Van Leer, Towards the ultimate conservative difference scheme. II. Monotonicity and conservation combined in a second-order scheme, Journal of Computational Physics. 14 (1974) 361–370.
[42] P. Kent, B.R. Saunders, The Role of Added Electrolyte in the Stabilization of Inverse Emulsions, Journal of Colloid and Interface Science. 242 (2001) 437–442. doi:10.1006/jcis.2001.7792.
[43] F. Michaut, P. Perrin, P. Hébraud, Interface Composition of Multiple Emulsions: Rheology as a Probe, Langmuir. 20 (2004) 8576–8581. doi:10.1021/la048715t.
[44] Theodore Vermeulen, Interfacial area in liquid-liquid and gas-liquid agitation, Chem. Eng. Progr. 51 (1955) 85F-94F.
[45] S. Okazaki, M. Imai, M. Shimizu, Leakage Suppressing Oe W/O Emulsion Using High Viscous Solvent, in: Process Metallurgy, Elsevier, 1992: pp. 1487–1492. doi:10.1016/B978-0-444-88677-4.50064-7.
[46] P. Julian Becker, F. Puel, H.A. Jakobsen, N. Sheibat-Othman, Development of an improved breakage kernel for high dispersed viscosity phase emulsification, Chemical Engineering Science. 109 (2014) 326–338. doi:10.1016/j.ces.2014.02.008.

Table 1: Effect of some process parameters on the swelling rate, permeability and lag time

	Effect on swelling / shrinkage rate	**Effect on L_p**	**Effect on lag time**	**Reference**
$\uparrow \phi_{\mu}$	-	No effect	-	Matsumoto et al. [26]
	$\downarrow$	$\downarrow$	-	Yan and Pal [30]
	No effect	-	$\downarrow$	Bahtz et al. (2015) [31]
$\uparrow \phi_{\text{ions}}$ (or $\uparrow \Delta\Pi$)	$\uparrow$	~No effect	No effect	Bahtz et al. (2015) [31]
	$\uparrow$	$\downarrow$	-	Matsumoto & Kohda [25]
$\uparrow \phi_{\text{emulsifier}}^{\text{in}}$	-	$\downarrow$	-	Matsumoto et al.[14, [26]
	-	$\uparrow$	-	Yan & Pal [30] Garti et al. (1985) [29]
	$\uparrow$	-	$\uparrow$	Jager-Lezer (1997) [15]
$\uparrow$ Oil viscosity	$\downarrow$	-	$\uparrow$	Bahtz et al. (2015) [31]
	$\downarrow$	$\downarrow$	-	Matsumoto et al. [26]
$\uparrow$ Temperature	$\uparrow$	No effect	$\downarrow$	Bahtz et al. (2015) [31]

Table 2: Experimental conditions

	First preparation step						Second preparation step					Right after preparation
	Operating parameters		Fractions (wt. %)				Operating parameters		Fractions (wt. %)			Encapsulation efficiency (%)
	t_1* (min)	ω_{R1}** (rpm)	Water	Mineral oil	NaCl	$Span_{80}$	t_2* (min)	ω_{R2}** (rpm)	Primary	Water	$Tween_{80}$	
Set 1 ϕ_M	4	12000	40	50	0.05	9.95	70	400	1	98	1	92.5
									2	97		94.7
									3	96		95.44
									4	95		95.5
Set 2 ϕ_{NaCl}	4	12000	40	50	0.05	9.95	70	400	1	98	1	92.5
					0.14							96.1
					0.19							96.4
					0.24							96.4
Set 3 ϕ_μ	4	12000	10	80	0.05	9.95	70	400	1	98	1	51.2
			20	70								67
			30	60								82.2
			40	50								92.5
Set 4 ω_R	4	12000	40	50	0.05	9.95	70	300	1	98	1	94.1
								350				93.3
								400				92.5
								500				88.1

*t_1 and t_2 are the mixing times of the first and second step respectively.

**ω_{R1} and ω_{R2} are mixing rates of the first and second emulsions respectively.

The total mass in the second step is 1 kg.

Table 3: Coalescence-driven escape models of inner droplets, with: $\frac{\mathrm{d}n_\mu}{\mathrm{d}t} = -\Omega_{\mathrm{es}}\, n_\mu^{cr}\, P$.

Pays et al. (2001) [21]**: Based on an adsorption isotherm**

Only droplets adsorbed on the surface (n_μ^{cr}) may escape, evaluated using the isotherm:

$\frac{\Theta}{1-\Theta} = \frac{1}{4}\pi d_\mu^2 \tau \mathrm{k_B}\, T \frac{(n_\mu - n_\mu^{\mathrm{cr}})}{\sqrt{2\pi m_\mu \mathrm{k_B} T}} \exp\left(\frac{u_\mathrm{a} + 4\, u_\mathrm{l}\, \Theta}{\mathrm{k_B}\, T}\right)$

With $\Theta = \frac{n_\mu}{n_0}$, $n_0 = d_\mathrm{M}^2/(d_\mu^2 v_\mathrm{M})$, $u_\mathrm{a} = \frac{1}{12 l_s} \mathrm{A_H} d_\mu$ and $u_\mathrm{l} \approx \frac{1}{24\, l_s} \mathrm{A_H} d_\mu$.

The escape frequency Ω_{es} is fitted to experimental data.

The escape probability is $P = 1$.

Klahn et al. (2002) [23]**: Double emulsions in simple shear flow**

The escape probability is assumed equal to the coalescence probability and is given by:

$P = \exp\left(\frac{t_\mathrm{d}}{t_\mathrm{i}}\right) \approx \left(\frac{\pi \sigma_{\mu,\mathrm{M}}}{6\mathrm{A_H}}\right)^{-\frac{4}{9\pi\tau_c}\left(1+\frac{\eta_\mathrm{M}}{\eta_\mathrm{out}}\right)}$

The volume fraction (with $n_\mu^{cr} = \alpha_{\mathrm{cr}}\, n_\mu$) is obtained by fitting to experimental data, giving:

$\alpha_{\mathrm{cr}} = 1 - \exp\left(-\frac{d_\mu}{d_\mathrm{M}}\left[2.22 + 1.51\left(\frac{\eta_\mathrm{M}}{\eta_\mathrm{out}}\right)^{-0.57}\right]\right)$

The escape frequency is obtained from the circulation time in a simple shear flow ($\tau_c = \frac{\dot{\gamma}}{4\pi} t_c$):

$\Omega_{\mathrm{es}} = \frac{2}{t_c}$

Chávez-Páez et al. (2012) [16]**: Based on 3D Brownian dynamics**

The global frequency of collisions of inner droplets with the surface of outer droplets (i.e. $\Omega_{\mathrm{es}}\, n_\mu^{cr}$) is determined by the equation of motion:

$r_i(t + \Delta t) = r_i(t) + \beta\, D_i\, F_i(t) \Delta t + R_i$

The interaction between particles is modelled by a short-range repulsive potential:

$\beta u_{ij}(r) = \varepsilon \exp(-z\,(r - L_{ij}))$, with $\beta = (k_B T)^{-1}$

The coalescence probability, P, is assumed to be determined by another source.

Kang et al. (2016) [24]**: Based on momentum and energy conservation**

The escape frequency is calculated from the dewetting time (See equations 9-13).

Table 4: Identified model parameters compared to literature values

Hydraulic permeability coefficient	**Volume fraction of the critical region, α_{cr}**	**Conditions**	**Reference**
2.75×10^{-15}	3.6×10^{-5}	Storage ($P = 1$)	This work
$2.27 \times 10^{-15} – 2.27 \times 10^{-14}$	-	Storage	Matsumoto & Kohda (1980) [25]
$2.27 \times 10^{-15} – 4.78 \times 10^{-15}$	-	Storage	Garti et al. (1985) [29]
$0.3 \times 10^{-15} – 5.87 \times 10^{-15}$	-	Storage	Yan & Pal (2001) [30]
$2.2 \times 10^{-14} – 2.72 \times 10^{-14}$	-	Storage	Bahtz et al. (2015) [31]
-	≈ 0.57	Storage (high escape rate, $P = 1$)	Pays et al. [21]
-	≈ 0.2	Simple Shear flow (with a probability term)	Klahn et al. [23]

P_0: Permeation coefficient (m s^{-1}), $L_p = \frac{P_0 V_w^*}{R T}$, V_w^*: Molar volume of pure water (m^3 mol^{-1})

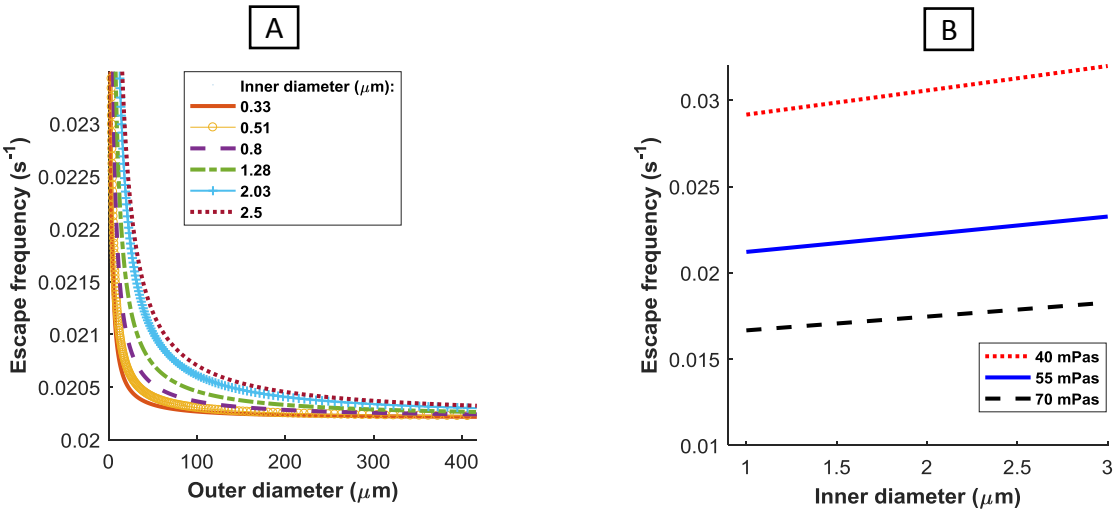

Figure 1: Escape frequency calculated by the dewetting model for: A) Different inner droplets diameters using η_M = 55 mPa s and $\sigma_{\mu,M} = 5 \times 10^{-3}$ N m^{-1}, and B) Different outer phase viscosities using $\sigma_{\mu,M} = 5 \times 10^{-3}$ N m^{-1} and d_M = 20 µm.

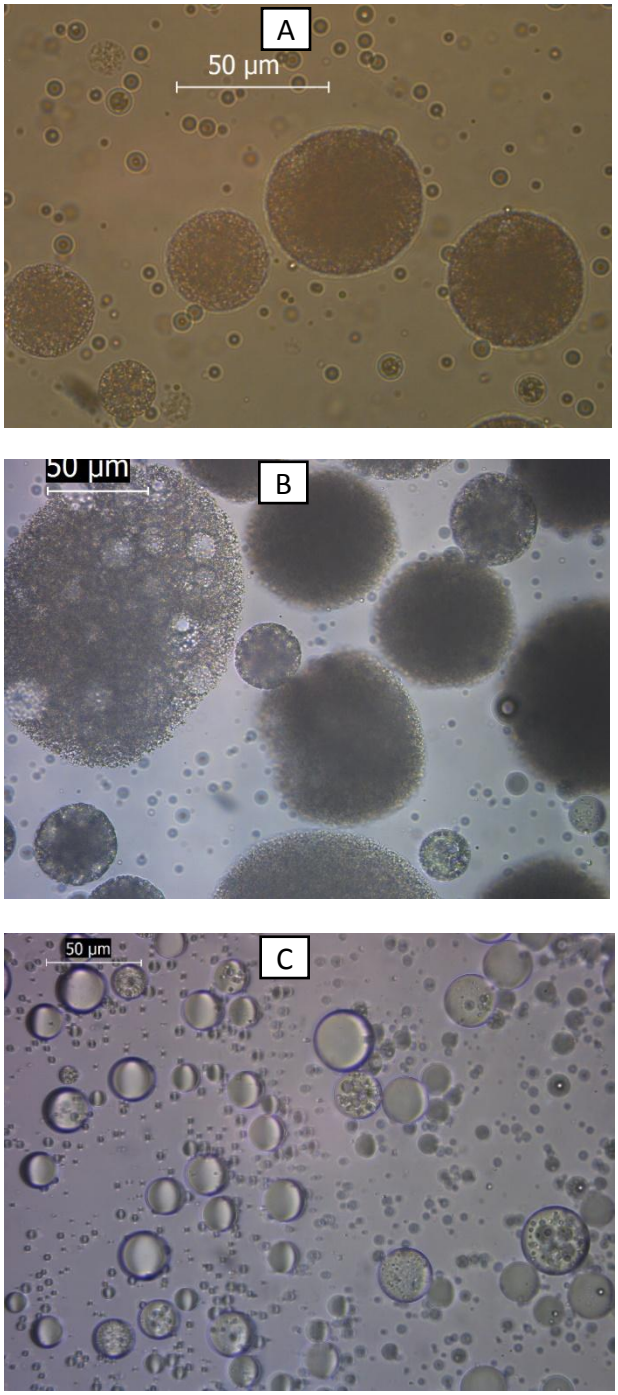

Figure 2: Microscopic images of the double emulsion prepared with ϕ_{μ} 40 %, ϕ_{M} = 1 %, and ω_{R} = 400 rpm: A) day 0 so right after preparation, B) day 6 and C) day 20.

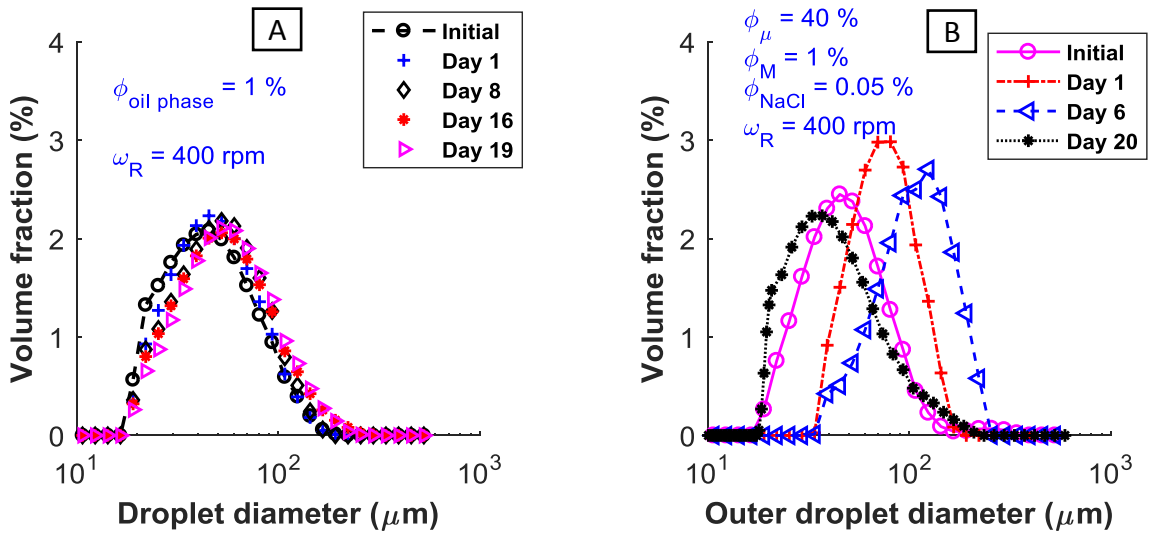

Figure 3: A) DSD of a single O/W emulsion. B) DSD of a double emulsion W/O/W. In both cases, similar fractions and mixing rates were employed, the oil phase consists of mineral oil and Span 80 and the external water phase consists of water and Tween 80.

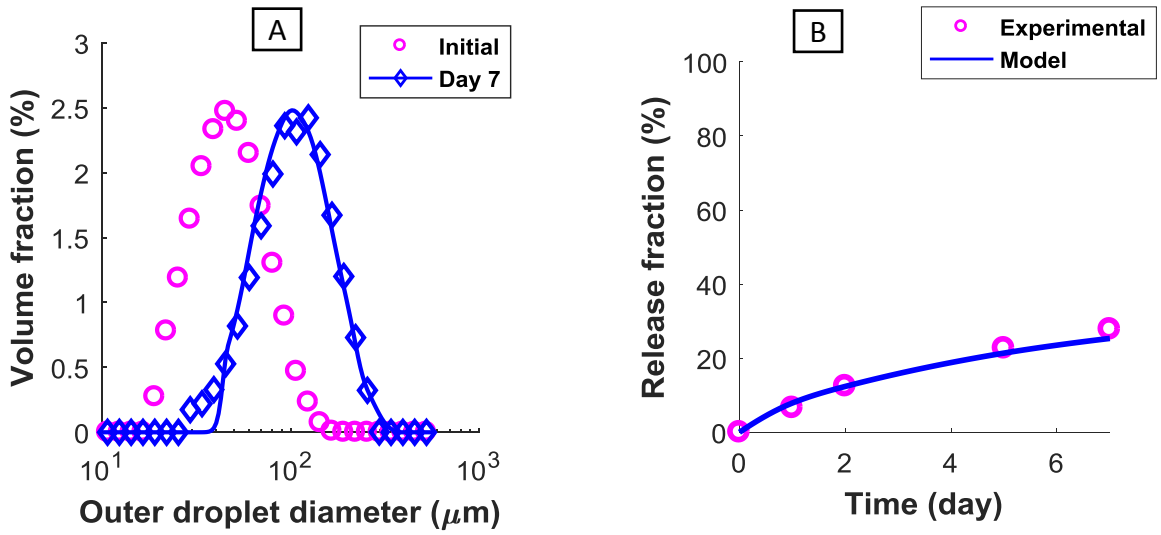

Figure 4: Results of the double emulsion prepared with ϕ_{μ} = 40%, ϕ_{M} = 4% and ω_{R} = 400 rpm. Experimental data is represented by the symbols and modelling results by the continuous lines. A) Outer DSD. B) Released fraction due to inner droplets escape.

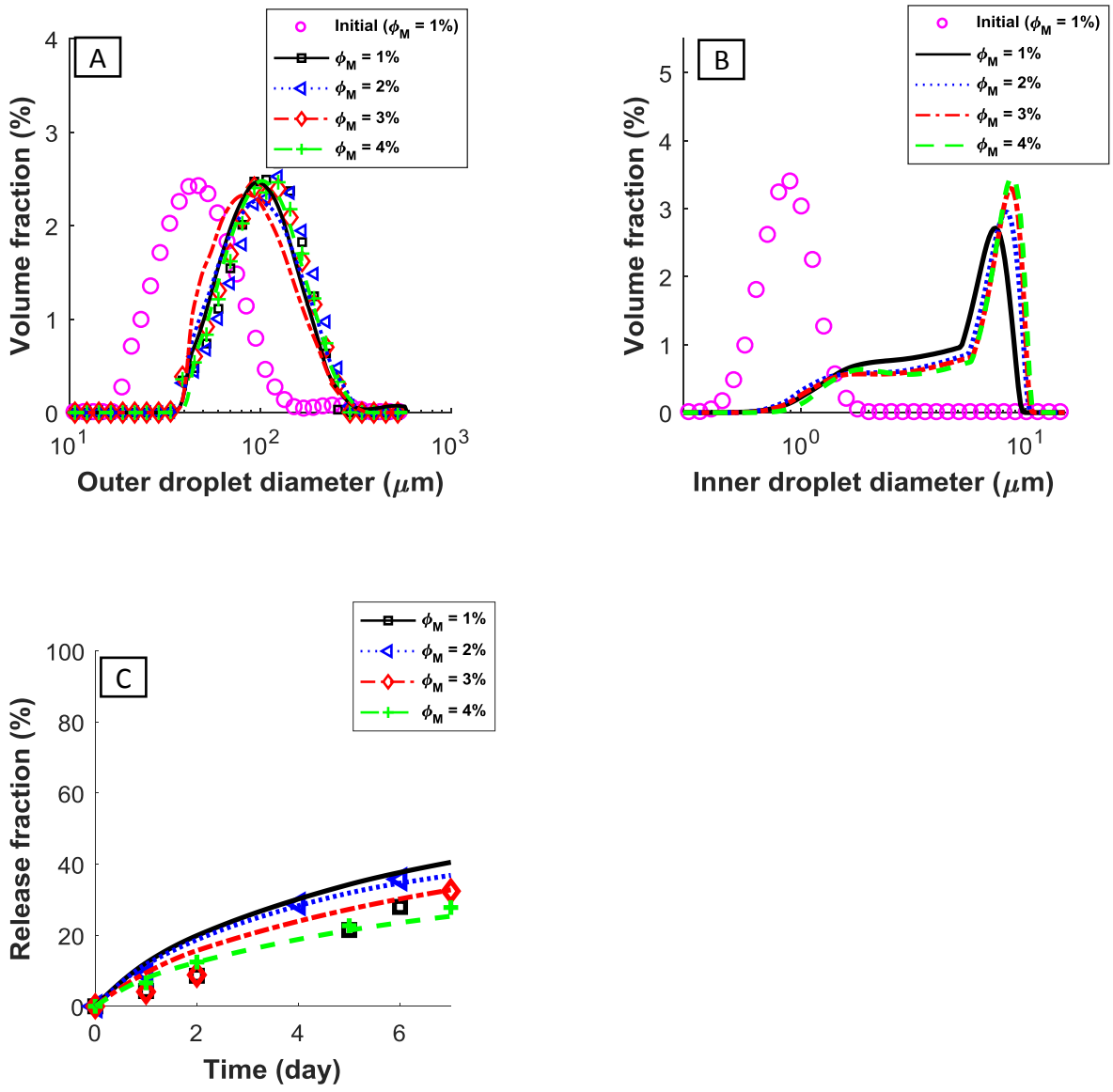

Figure 5: Effect of the primary emulsion fraction (ϕ_M). A) Outer DSD at day 0 and after one week of storage. B) Inner DSD at day 0 and after one week of storage. C) Released fraction over one week of storage. The lines indicate the model predictions and the symbols the experimental measurements.

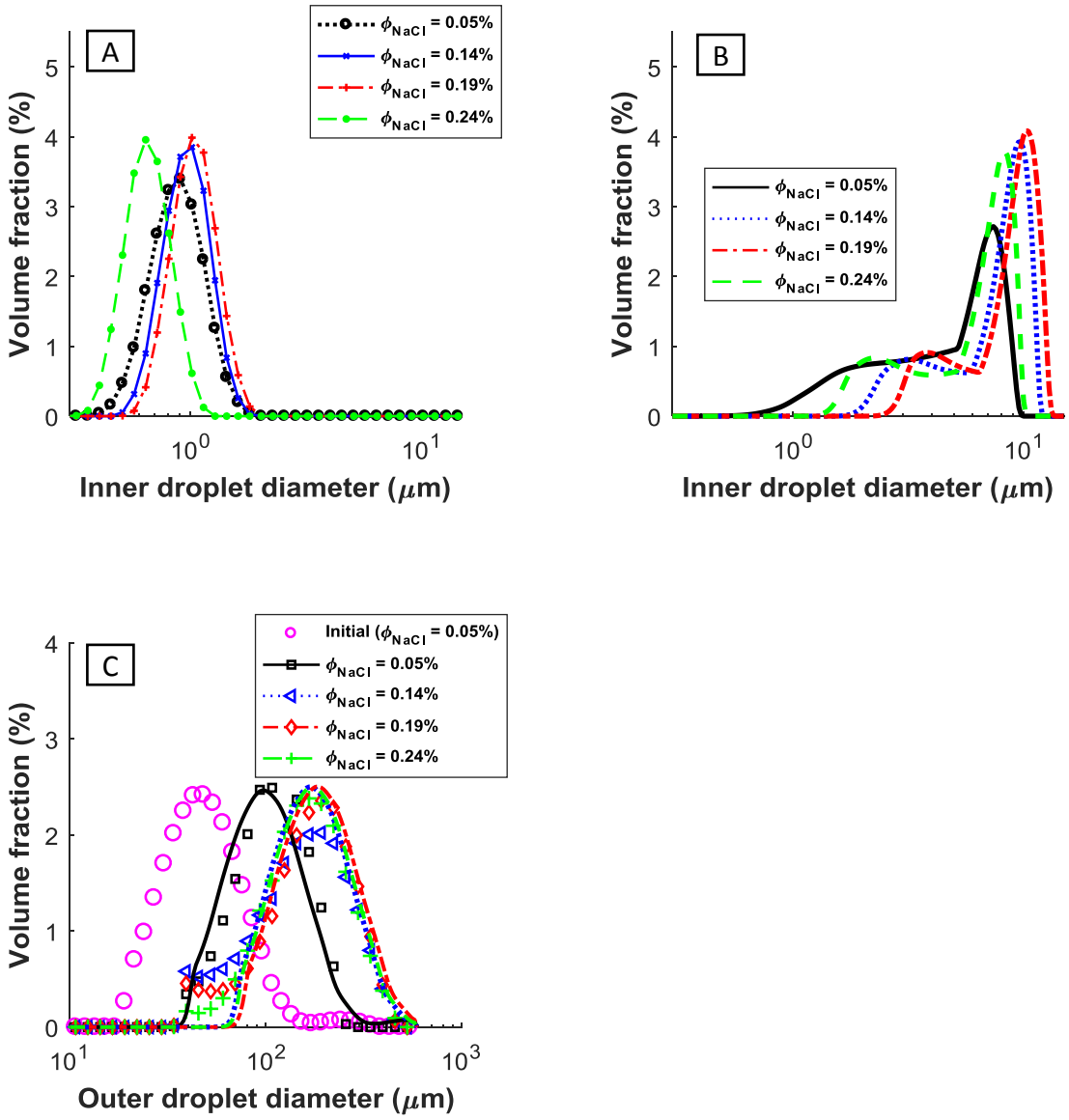

Figure 6: Effect of the salt fraction (ϕ_{NaCl}). A) Measured initial inner DSD (after the 1st preparation step). B) Model prediction of the inner DSD after one week of storage. C) Outer DSD (initial and after one week of storage) by the model (represented by the continuous lines) and experimentally (symbols).

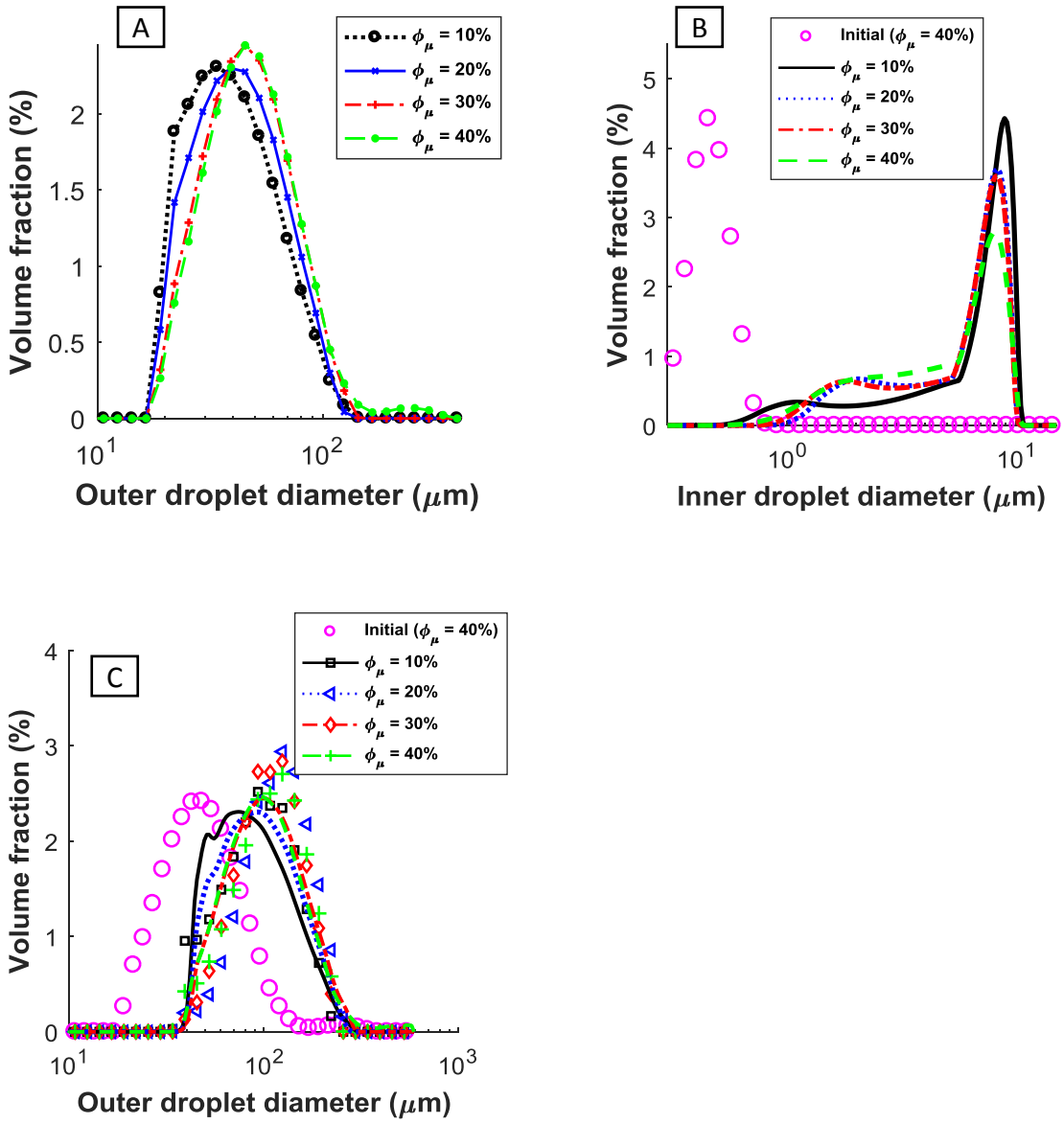

Figure 7: Effect of the internal phase fraction (ϕ_μ). A) Measured outer DSD at day 0 (after the 2nd preparation step). B) Measured initial inner DSD and predicted after one week. C) Outer DSD (initial and after one week), where the lines indicate the model predictions and the symbols the experimental measurements.

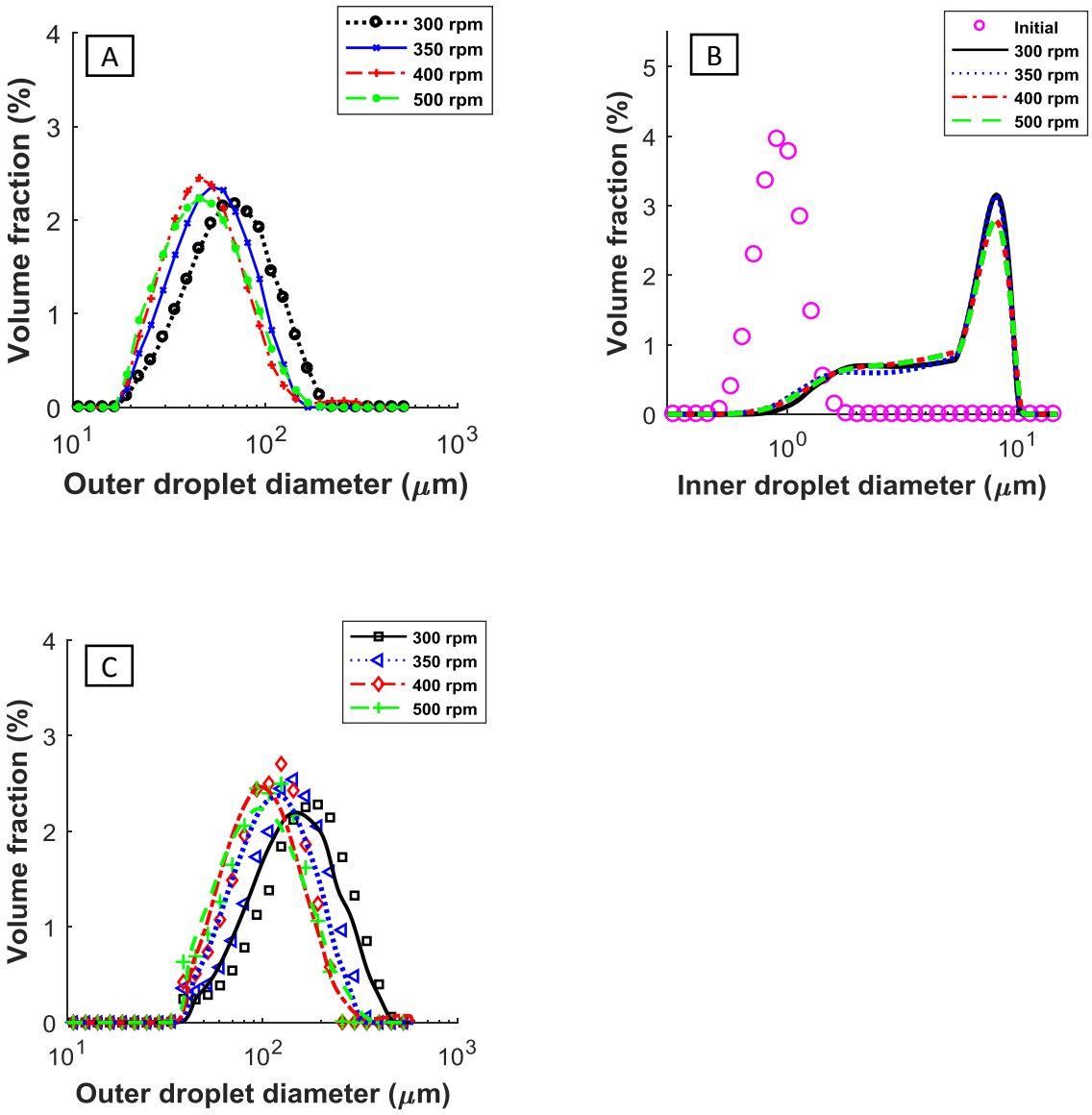

Figure 8: Effect of the stirring rate (ω_R) in the 2nd preparation step. A) Measured outer DSD at day 0. B) Inner DSD (initial-experimental; and after one week using the storage model). C) Outer DSD after one week of storage, where the continuous lines indicate the model predictions and the symbols the experimental measurements.

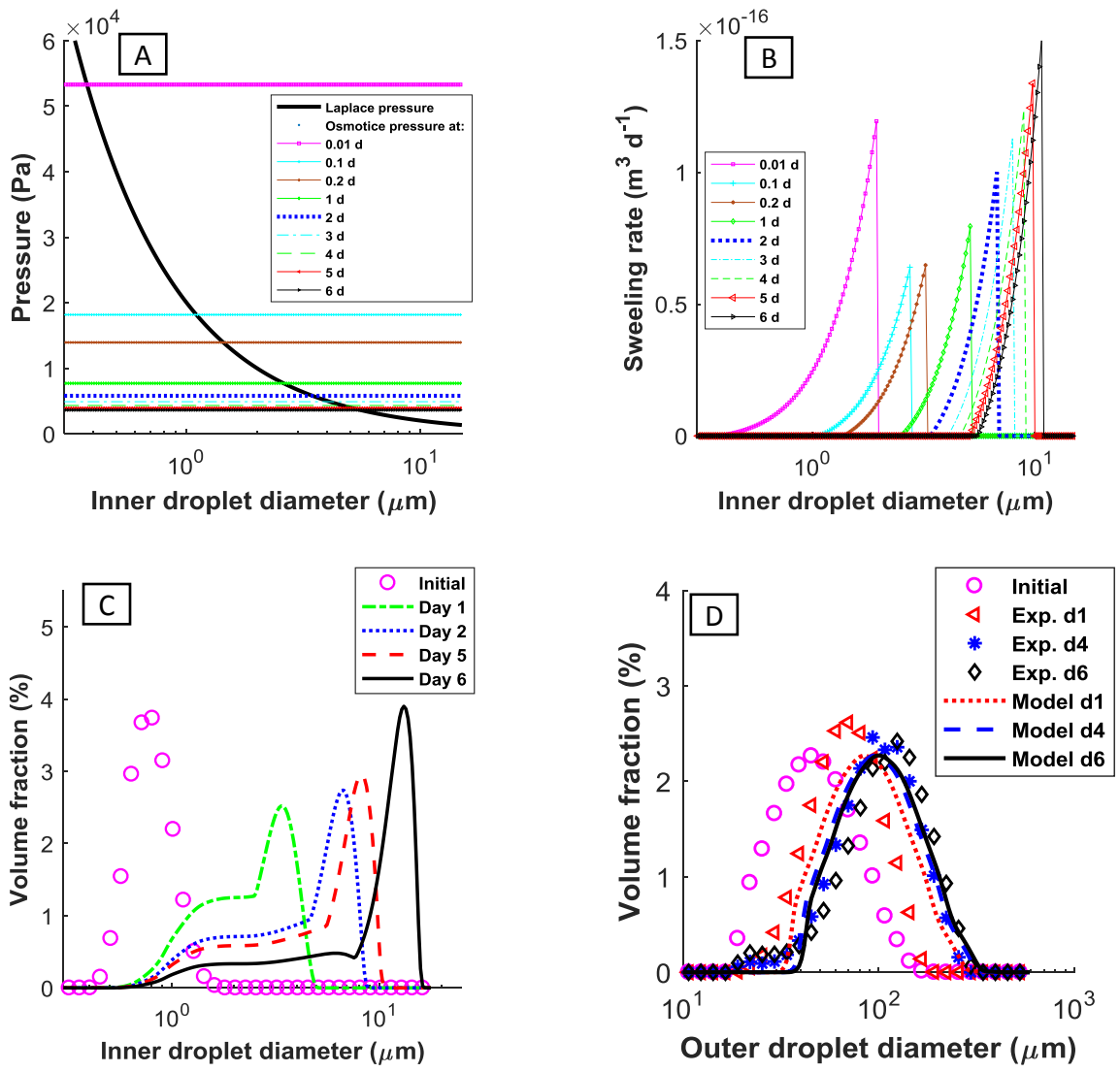

Figure 9: Swelling during storage (sample prepared with ϕ_μ = 40 %, ϕ_M =2 %, and ω_R=400 rpm). A) Osmotic and Laplace pressures. B) Swelling rate (eq. 3) of the inner droplets ($\mathbb{S}_\mu = 0$ if $n_\mu = 0$ or $\Delta\Pi < \Delta P(v_\mu)$). C) Inner DSD. D) Outer DSD. The lines indicate the model predictions and the symbols the experimental measurements.